Inorg. Chem. **2007**, *46*, 965–974

Redox Behavior of Phenyl-Terpyridine-Substituted Artificial Oligopeptides Cross-Linked by Co and Fe

Kristi Ohr, Rebekah L. McLaughlin, and Mary Elizabeth Williams*

Department of Chemistry, The Pennsylvania State University, 104 Chemistry Building, University Park, Pennsylvania 16802

Received July 1, 2006

This work presents the synthesis and characterization of metalated oligopeptide duplex assemblies composed of artificial oligopeptides bearing tethered phenyl terpyridine ligands that are coordinated to Co(II) and Fe(II) ions. The metals cross-link the oligopeptide strands, forming duplex structures. UV–vis spectrophotometric titrations that monitor the absorbance of the metal complexes' characteristic MLCT bands demonstrate stoichiometric metal chelation. Anodic peaks in the cyclic voltammograms of these molecules are consistent with one-electron oxidative reactions without strong coupling between the metal complexes. In separate chronocoulometry measurements, the diffusion coefficients of the metal complexes decrease with increasing oligopeptide length, suggesting the primary products are metal-linked oligopeptide duplex assemblies. Larger metalated oligopeptides adsorb to electrode surfaces during cyclic voltammetry and yield irreversibly adsorbed electroactive films with thicknesses that depend on the number of voltage cycles. Electrochemical and spectroelectrochemical investigations of the films on Pt and ITO electrodes show that the electron transfers in the adsorbed films are chemically reversible but are kinetically quasi-reversible.

Introduction

Over the past 30 years[1] the burgeoning field of molecular electronics has encompassed materials ranging from conducting polymers[2] to porphyrin-based multichromophore assemblies[3] to self-assembled monolayers[4] to be utilized in the construction of wires, switches, and gates. Double-stranded DNA (dsDNA) is a particularly attractive candidate for molecular wires because its self-recognition is ideally suited for bottom-up construction of potentially long, linear structures.[5] The incorporation of metal atoms into the dsDNA duplex[6] (or even the peptide nucleic acid, PNA, analogs[7]) might be expected to increase the number of addressable redox couples, improve electron transport kinetics, and improve the conductivity of dsDNA by insertion of redox sites. However, metal ion chelation with nucleic acids and the phosphoester backbone is known to occur, which would create defect sites along the desired molecular wire. In addition, the redox chemistry of nucleic acids limits the accessible voltage range that can be applied since irreversible oxidative cleavage occurs at anodic potentials.[8] We have therefore sought to create analogous supramolecular struc-

* To whom correspondence should be addressed. E-mail: mbw@chem.psu.edu.

(1) Aviram, A.; Ratner, M. A. *Chem. Phys. Lett.* **1974**, *29*, 277−283.
(2) (a) Schennig, A. P. H. J.; Meijer, E. W. *Chem. Commun.* **2005**, *26*, 3245−3258. (b) Roncali, J. *Acc. Chem. Res.* **2000**, *33*, 147−156. (c) Tour, J. *Chem. Rev.* **1996**, *96*, 537−553.
(3) (a) Zhang, T.-G.; Zhao, Y.; Asselberghs, I.; Persoons, A.; Clays, K.; Therien, M. J. *J. Am. Chem. Soc.* **2005**, *127*, 9710−9720. (b) Gust, D.; Moore, T. A.; Moore, A. L. *Chem. Comm.* **2006**, *11*, 1169−1178. (c) Carcel, C. M.; Laha, J. K.; Loewe, R. S.; Thamyongkit, P.; Schweikart, K.-H.; Misra, V.; Bocian, D. F.; Lindsey, J. S. *J. Org. Chem.* **2004**, *69*, 6739−6750.
(4) (a) Tour, J. M.; James, D. K. *Chem. Mater.* **2004**, *16*, 4423−4435. (b) Wang, W.; Lee, T.; Reed, M. A. *Proc. IEEE* **2005**, *93*, 1815−1824.
(5) (a) Taniguchi, M.; Kawai, T. *Physica E* **2006**, *33*, 1−12. (b) Berlin, Y. A.; Burin, A. L.; Ratner, M. A. *Superlattices Microstruct.* **2000**, *28*, 241−252. (c) Endres, R. G.; Cox, D. L.; Singh, R. R. P. *Rev. Mod. Phys.* **2004**, *76*, 195−214.
(6) (a) Meggers, E.; Holland, P. L.; Tolman, W. B.; Romesburg, F. E.; Schultz, P. G. *J. Am. Chem. Soc.* **2000**, *122*, 10714−10715. (b) Weizman, H.; Tor, Y. *J. Am. Chem. Soc.* **2001**, *123*, 3375−3376. (c) Artwell, S.; Meggers, E.; Spraggon, G.; Schultz, P. G. *J. Am. Chem. Soc.* **2001**, *123*, 12364−12367. (d) Tanaka, K. Yamada, Y.; Shionoya, M. *J. Am. Chem. Soc.* **2002**, *124*, 8802−8803. (e) Tanaka, K.; Tengeiji, A.; Kato, T.; Toyama, N.; Shiro, M;, Shionoya, M. *J. Am. Chem. Soc.* **2002**, *124*, 12494−12498.
(7) (a) Popescu, D.; Parolin, T. J.; Achim, C. *J. Am. Chem. Soc.* **2003**, *125*, 6354−6355. (b) Mokhir, A.; Stiebig, R.; Kraemer, R. *Bioorg. Med. Chem. Lett.* **2003**, *13*, 1399−1401. (c) Watson, R. M; Skorik, Y. A.; Patra, G. K.; Achim, C. *J. Am. Chem. Soc.* **2005**, *127*, 14628−14629.
(8) (a) Schuster, G. B. *Acc.Chem. Res.* **2000**, *33*, 253 − 260. (b) O'Neill, M. A.; Barton, J. K. *J. Am. Chem. Soc.* **2004**, *126*, 11471 − 11483.

10.1021/ic0612101 CCC: $37.00
Published on Web 01/05/2007

Scheme 1. Representation of Metal-Chelation-Based Molecular Recognition of Artificial Oligopeptide Strands: (A) Tridentate−Monodentate and (B) Bidentate−Bidentate Ligand Pairs Are Selectively Linked by Tetracoordinate Metals. (C) the Tridentate−Tridentate Ligand Pair Is Cross-linked by Hexacoordinate Metals.

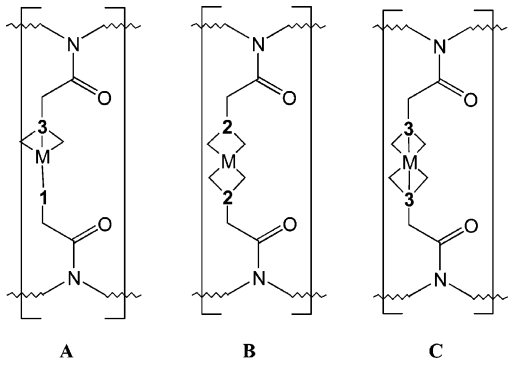

tures that self-assemble solely upon metal chelation, creating more robust bonds and less dynamic structures than DNA and PNA, while simultaneously providing accessible and reversible electron-transfer pathways.

In our inorganic self-assembly motif, molecular recognition between artificial oligopeptides is achieved when the denticity of the ligands provide coordinative saturation for a metal ion. For example, tetracoordinate metals would be expected to form interstrand links between oligopeptides containing bidentate ligands (i.e., 2×2) or a monodentate and a tridentate ligand (i.e., 1×3) (Scheme 1A and B). Six-coordinate metals would instead cross-link oligopeptides containing tridentate ligands (e.g., 3×3) as in Scheme 1C. Selective crosslinking of two strands in this manner is analogous to base pairing in DNA: by tethering "complementary" ligands to oligopeptides, metal chelation forms double-stranded structures. The artificial oligopeptides are scaffolds that hold these complexes in a geometry that should enable electron transfers between proximal metals; the metal-linked oligopeptide duplexes can thus serve as model molecular wires.

We have recently reported the synthesis of a series of ligand-substituted oligopeptides[9] based on an aminoethylglycine (aeg) backbone, which is superior to the phosphoester framework of DNA in terms of enhanced stability and solubility in a variety of environments and lower affinity with metal species.[10] These artificial oligopeptides were used to stoichiometrically complex metals and form supramolecular structures; double-stranded duplexes formed when bipyridine-containing artificial tripeptides were crosslinked by Cu(II) ions.[9a] While these metal−oligopeptide assemblies possess unique spectroscopic[9a] and electrochemical properties[9a,b,d] that are dictated by the identities of the metal and ligand and the oligopeptide length, the slow electron-transfer kinetics of the Cu(II/I) reaction limits the use of that peptide duplex. To study the dynamics of transport in these one-dimensional molecular wires, different redox centers with a range of electron-transfer rates and formal potentials are necessary.

We have therefore begun to incorporate six-coordinate metals, with their well-known rich and widely varying redox chemistry, into the double-stranded oligopeptide scaffolds. To accomplish this, new artificial oligopeptides containing the tridentate ligand phenyl terpyridine (Scheme 2) have been prepared. These are reacted with either Co(II) or Fe(II) to create metal bis(phenyl terpyridine) complexes that cross-link the peptide strands. This paper presents the synthesis and characterization of the oligopeptides and their Fe and Co complexes and investigates their solution and film electrochemical and spectroelectrochemical behavior as a function of the length (i.e., number of metals) of the oligopeptides. These experiments represent the first demonstration of these inorganic DNA mimics as electrochemically and chemically reversible structures and pave the way to their use as molecular wires.

Experimental Section

Chemicals. All materials were reagent grade, purchased from Acros, and used as received unless otherwise noted. Water was obtained from a nanopure water system (Barnstead, 18.2 MΩ). *N*′,*N*-Diisopropylethylamine (DIPEA) and acetonitrile (ACN) were distilled over CaH_2 under N_2. Tetrabutylammonium perchlorate (TBAP) was recrystallized 3× from ethyl acetate and dried in vacuo. Ferrocene (Fc) was purified by sublimation.

Instrumentation and Analysis. Preparatory and analytical scale reverse-phase high performance liquid chromatographies (HPLC) were performed with a Varian system equipped with two quaternary pumps (Model 210), an autosampler (Model 410), a UV−vis detector (Model 320), a fraction collector (Model 701), and C-18 columns. Oligomer elution was monitored at 254 nm.

The UV−vis absorption spectra were obtained with a double-beam spectrophotometer (Varian, Cary 500). Positive-ion electrospray mass spectrometry (ESI+) was performed at the Penn State Mass Spectrometry Facility using a Mariner mass spectrometer (Perseptive Biosystems.) All NMR spectra were collected on either 300 or 400 MHz spectrophotometers (Bruker). Diffuse reflectance infrared spectra were collected on a Varian FTS 7000 spectrophotometer using KBr.

All solution-phase electrochemical measurements were obtained with a CH Instruments potentiostat (Model 660) with a 0.22 cm diameter Pt working and Pt wire counter electrodes with a Ag/Ag^+ reference electrode. Solutions were prepared from distilled ACN containing 0.15 M TBAP supporting electrolyte and 20% H_2O. After voltammograms were obtained, Fc was added as an internal potential reference to convert to the SCE scale.[11]

Electrochemical analysis of films was conducted on either 0.22 cm diameter Pt or indium−tin oxide (ITO) coated glass working electrodes with Pt wire counter and Ag/Ag^+ reference electrode. Following film deposition, the coated electrodes were washed copiously with ACN and immersed in solutions containing only supporting electrolyte (0.2 M TBAP in ACN) for electrochemical and spectroelectochemical measurements.

(9) (a) Gilmartin, B. P.; Ohr, K.; McLaughlin, R. L., Koerner, R.; Williams, M. E. *J. Am. Chem. Soc.* ***2005***, *127*, *9546*−9555. (b) Ohr, K.; Gilmartin, B. P.; Williams, M. E. *Inorg. Chem.* **2005**, *44*, 7876−7885. (c) Levine, L. A.; Morgan, C. M.; Ohr, K.; Williams, M. E. *J. Am. Chem. Soc.* **2005**, *127*, 16764−16765. (d) Gilmartin, B. P.; McLaughlin, R. L.; Williams, M. E. *Chem. Mater*. **2005**, *17*, 5446−5454.

(10) Barton, J. K.; Lippard, S. J. Nucleic Acid-Metal Ion Interactions. In *Metal Ions in Biology*; Spiro, T. G., Ed.; John Wiley and Sons: New York, 1980; Vol. 1, pp 32−113.

(11) Bard, A. J.; Faulkner, L. R. *Electrochemical Methods, Fundamentals and Applications*, 2nd ed.; John Wiley and Sons: New York, 2001.

Scheme 2. Monomer Synthesis[a]

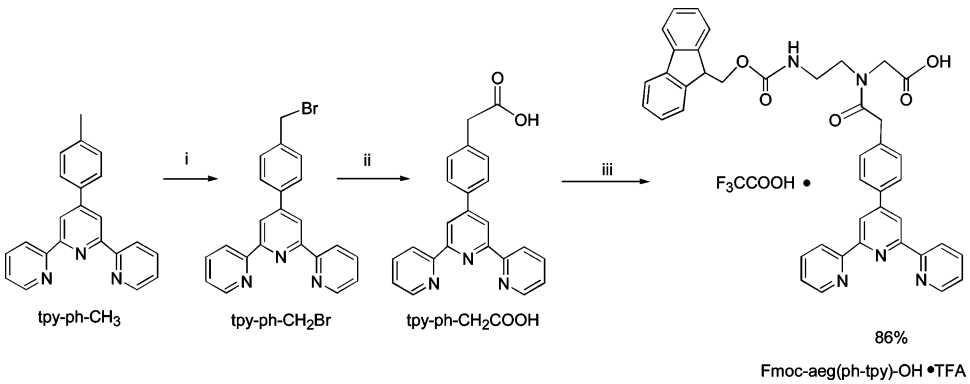

[a] (i) NBS, AIBN, benzene; (ii) 1. NaCN, DMSO, 2. conc HCl; (iii) 1. Fmoc-aeg-otBu, EDC, HOBt, DIPEA, CH_2Cl_2, 2. 2.5% triisopropylsilane in TFA.

Synthesis. ***Caution:*** *Perchlorate salts are potentially explosive and should be handled with care!* The syntheses of *N*-[2-(Fmoc aminoethyl]glycinate *t*-butylester hydrochloride (Fmoc-aeg-OtBu·HCl)[12] and 4′-(4-bromomethyl-phenyl)-[2,2′;6′2″]terpyridine (tpy-ph-CH_2Br)[13] have been previously reported.

4′-*p*-Tolyl-[2,2′;6′,2″]terpyridine (tpy-ph-CH_3). The synthesis of tpy-ph-CH_3 follows a modified literature preparation.[14] *p*-Tolualdehyde (14 mL, 0.12 mol, Alfa Aesar), 2-acetylpyridine (29 mL, 0.26 mol), 200 mL of methanol, 200 mL of concentrated ammonium hydroxide, and 20 mL of 15% KOH were refluxed for 2 days. The mixture was cooled to room temperature, diluted with water (300 mL), and extracted with ether (6 × 200 mL.) The combined ether layers were extracted with water (2 × 100 mL) and evaporated to yield a brown sludge. The product was isolated as white crystals by recrystallization from 95:5 ethanol/water. Yield = 22.2 g (58.1%) ^{1}H NMR (300 MHz, d_6-DMSO): 2.31 (s, 3H), 7.30 (d, 2H, J = 6 Hz), 7.42 (t, 2H, J = 6 Hz), 7.75 (d, 2H, J = 12 Hz), 7.95 (t, 2H, J = 15 Hz), 8.51 (d, 2H), 8,56 (s, 2H), 8.67 (d, 2H).

(4-[2,2′;6′,2″]Terpyridin-4′-yl-phenyl)-acetic Acid (tpy-ph-CH_2COOH). A 7.42 g amount of tpy-ph-CH_2Br (0.0185 mol) and 5.00 g of NaCN (0.102 mol) in 125 mL of DMSO were stirred at 70 °C for 18 h. The mixture was cooled to room temperature, and unreacted NaCN was decomposed by addition of concentrated HCl (ca. 10 mL). The mixture was brought to pH 7 with 6 M NaOH and poured over 600 g of ice. The resulting yellow precipitate was collected by filtration and washed with water. The solid was suspended in 50 mL of concentrated HCl and refluxed for 4 h. The mixture was poured over ice water (500 mL) and brought to pH 5 with 6 M NaOH. The tan solid was collected, rinsed with water, isopropanol, and ether, and then dried at 100 °C in vacuo for 24 h. Yield = 5.14 g (75.9%) ^{1}H NMR (300 MHz, d_6-DMSO): 3.59 (s, 2H), 7.41 (d, 2H), 7.50 (t, 2H), 7.87 (d, 2H, J = 15 Hz), 8.02 (t, 2H, J = 9 Hz), 8.61 (d, 2H), 8.67 (s, 2H), 8.72 (d, 2H), 12.39 (s, 1H); FTIR (KBr, cm^{-1}): ν 2401−3552 (COOH), 2360 (COO), 2339 (COO), 1716 (C═O)

{**[2-(9*H*-Fluoren-9-ylmethoxycarbonylamino)-ethyl]-[2-(4-[2,2′;6′,2″]terpyridin-4′-yl-phenyl)-acetyl]-amino**}**-acetic acid, Trifluoroacetic Acid Salt (Fmoc-aeg(ph-tpy)-OH·TFA).** A 5.14 g quantity of tpy-ph-CH_2COOH (0.0140 mol), 2.75 g of EDC (0.0144 mol), and 2.01 g of HOBt (0.0149 mol) were suspended in 300 mL of CH_2Cl_2, and the mixture stirred for 15 min. Fmoc-aeg-OtBu·HCl (4.85 g, 0.0112 mol) was then added, followed by 8.0 mL of DIPEA (0.046 mol.) The mixture was allowed to stir for 24 h and then extracted with H_2O (3 × 100 mL). The organic layer was dried over anhyd Na_2SO_4, separated from the drying agent, and flash evaporated to yield a brown oil. The oil was

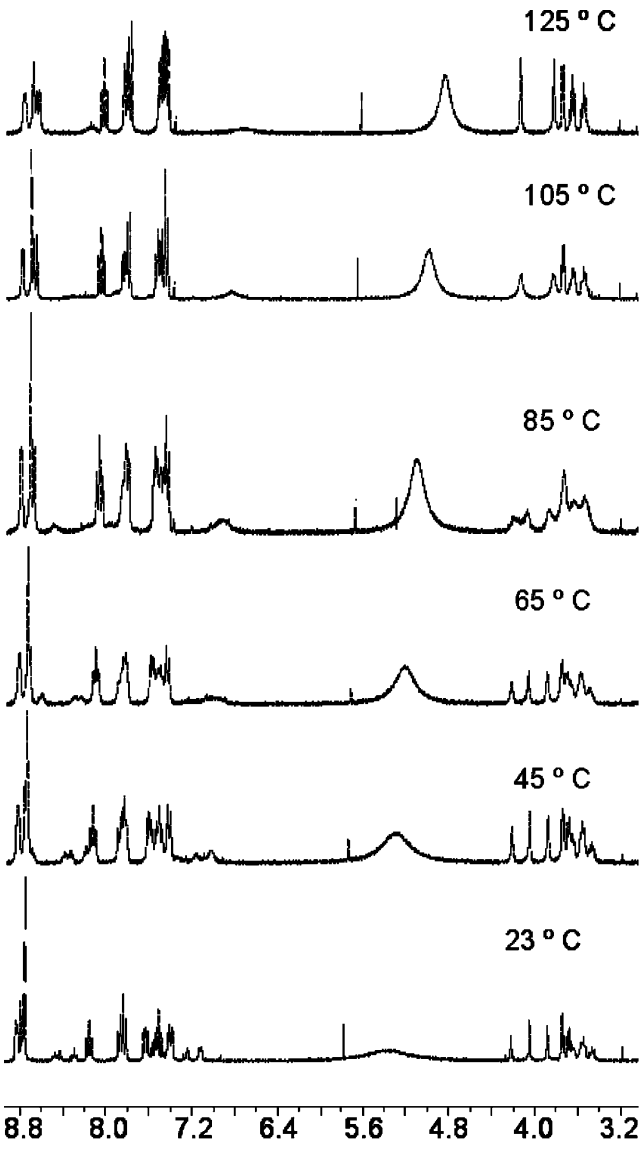

Figure 1. Temperature-dependent ^{1}H NMR (400 MHz) spectra of ***1*** in d_6-DMSO.

(12) Thompson, S. A.; Josey, J. A.; Cadilla, R.; Gaul, M. D.; Hassman, C. F.; Luzzio, M. J.; Pipe, A. J.; Reed, K. L.; Ricca, D. J.; Wiethe, R. W.; Noble, S. A. *Tetrahedron* **1995**, *51*, 6179−6194.
(13) (a) Collin, J. P.; Guillerez, S.; Sauvage, J. P.; Barigelletti, F.; De, Cola, L.; Flamigni, L.; Balzani, V. *Inorg. Chem.* **1991**, *30*, *4230*−4238. (b) Spahni, W.; Calzaferri, G. *Helv. Chim. Acta* **1984**, *67*, 450−454.
(14) Vaduvescu, S.; Potvin, P. G. *Eur. J. Inorg. Chem.* **2004**, *8*, 1763−1769.

Table 1. Phenyl Terpyridine-Substituted Oligopeptide Characterization Data

length	1	2	3	4
yield (mg)	30.7 (41.4%)	29.6 (22.7%)	41.0 (21.9%)	54.5 (22.4%)
ESI+ found (calcd)	628.2 (628.26)	1077.5 (1077.44)	1526.6 (1526.63)	1974.8 (1974.81)

chromatographed on a silica column eluting with a gradient (CH_2Cl_2 to 5% methanol in CH_2Cl_2). The tBu-protected product was isolated as the major band containing tpy. Following flash evaporation and drying in vacuo, the foam product was stirred in 2.5% triisopropylsilane in 20 mL of TFA for 3 h. The carboxylic acid product was obtained as a yellow powder by precipitation from 300 mL of sonicating ether, washed with ether, and drying in vacuo. Yield = 6.69 g (86.5%) ESI+: found (calcd) 690.27 (690.27) ^{1}H NMR (300 MHz, d_6-DMSO): 3.23 (bm, 2H), 3.51 (m, 2H), 3.79 (s, 1H), 3.91 (s, 1H), 4.05 (s, 1H), 4.32 (m, 2H), 4.41 (d, 1H), 7.32−7.60 (m−m, 7H), 7.75 (m, 5H), 7.92 (d, 4H), 8.28 (t, 2H), 8.88 (m, 6H): FTIR (KBr, cm^{-1}): ν 3333 (OH), 2389−3477 (COOH), 2359 (COO), 2333 (COO), 1651 (C═O).

Oligomer Synthesis. The oligomers ***1***−***4*** were prepared by hand via solid-phase peptide synthesis. The oligopeptides were prepared in DMF at a 0.1 mmol scale using Fmoc-PAL-PEG-PS resin (Applied Biosystems). Fmoc deprotection was performed for 15 min with 20% piperidine in DMF. Couplings were carried out using a 4-fold molar excess of monomers for 18 h with solutions of 0.5 M HBTU and 1 M DIPEA. Capping steps were performed after each coupling step using 0.5 M benzoic anhydride and 0.5 M DIPEA in DMF for 15 min.

Oligopeptides were cleaved from the resin using 2.5% triisopropylsilane and 2.5% water in TFA by stirring the resin for 3 h in this solution. Upon filtration into 160 mL of cold ether, the crude products were obtained as off-white precipitates. These were collected by centrifugation and washed with ether (3 × 40 mL). The oligopeptides were purified by preparatory scale reverse-phase HPLC by elution with a solvent gradient ramp of 15:85 to 37:63 (v/v of 0.1% TFA in ACN/0.1% aqueous TFA) for 25 min with a total flow rate of 5 mL/min. In each case, the oligopeptide was found to be the major peak. The oligopeptides were isolated as films following flash evaporation and were further dried by lyophilization (72 h) to yield off-white fluffy solids. Yields are provided in Table 1. The identity of the purified oligopeptides was confirmed with ESI+, and the calculated and observed *m*/*z* are also given in Table 1. Purity, identity, and dryness (following extensive lyophilization) were confirmed with ^{1}H NMR. Additional characterization was performed by HMQC NMR (Supporting Information) and variable-temperature ^{1}H NMR for ***1*** (Figure 1). ^{1}H NMR (400 MHz, d_6-DMSO): (***1***): 3.44 (m, 1H), 3.54 (m, 2H), 3.64 (m, 2.5H), 3.72 (m, 1.5H), 3.87 (s, 1H), 4.03 (s, 1H), 4.21 (s, 1H), 7.10 (m, 1H), 7.21 (bs, 0.5H), 7.39 (m, 2.5H), 7.50 (m, 3H), 7.62 (t, 2H), 7.83 (m, 4H), 8.14 (t, 2H), 8.28 (t, 0.5H), 8.42 (t, 0.5H), 8.48 (t, 0.5H), 8.75 (m, 4.5H), 8.82 (m, 2H); (***2***): 3.35−3.77 (m, 10H), 3.82−3.93 (m, 3H), 3.94−4.08 (m, 4H), 4.20 (m, 1H), 7.11 (m, 1H), 7.22 (bs, 0.5H), 7.26−7.60 (m, 12H), 7.61−7.90 (m, 6H), 7.93−8.13 (m, 4H), 8.23−8.37 (mm, 1.5H), 8.42−8.85 (m, 13H); (***3***): 3.21−3.71 (m, 16H), 3.75 (m, 2H), 3.85 (bs, 1H), 3.91 (bs, 1H), 4.04 (m, 4H), 4.20 (m, 2H), 7.12 (bs, 1H), 7.19−7.68 (m, 19H), 7.68−7.96 (m, 6.5H), 7.96−8.22 (m, 6.5H), 8.22−8.92 (m, 20H); (***4***): 3.21−3.77 (m, 19H), 3.80−4.25 (m, 15H), 7.12 (bs, 1H), 7.18−8.07 (m, 37H), 8.10−8.85 (m, 29H).

Metal Complexation. Following lyophilization, solutions of ***1***−***4*** were prepared in spectroscopic grade methanol (MeOH), and the phenyl terpyridine concentrations were determined from a calibration curve generated for the phenyl terpyridine monomer (Fmoc-aeg(ph-tpy)OH·TFA) as described previously,[9a] using its measured molar extinction value of 39540 M^{-1} cm^{-1} at 279 nm. The complexation of cobalt (II) perchlorate hexahydrate ($Co(ClO_4)_2 \cdot 6H_2O$, Aldrich) and iron (II) perchlorate hexahydrate ($Fe(ClO_4)_2 \cdot 6H_2O$, Aldrich) with each of the oligomers was monitored by UV−vis absorption spectroscopy at their respective MLCT bands, 514 and 567 nm. Solutions of metal complex in MeOH were prepared and the metal complex concentrations measured with their extinction coefficients (2.74×10^4 and 2.45×10^3 M^{-1} cm^{-1} for the Fe and Co species, respectively). For each experiment, the same metal solution was placed in the sample and reference cuvettes of a double beam spectrophotometer. The oligomer solution was then added in 25−50 μL increments to the sample beam cuvette; an equivalent volume of solvent was added to the reference cell. For each iterative addition, the solutions were stirred for a minimum of 5 min at room temperature, after which the UV−vis absorbance spectra were measured. The MeOH solutions of the metal−oligomer complexes were evaporated to dryness and lyophilized for a minimum of 72 h prior to electrochemical analysis and structural characterization. ESI+ found (calcd): $[Co(\mathbf{1})_2](ClO_4)_2$: M^{2+} = 656.7 (656.7); $[Co_2(\mathbf{2})_2](ClO_4)_4$: M^{4+} = 567.99 (567.69); $[Fe(\mathbf{1})_2](ClO_4)_2$: M^{2+} = 655.3 (655.2); $[Fe_2(\mathbf{2})_2](ClO_4)_2$: M^{4+} = 566.49 (566.19): ^{1}H NMR (400 MHz, d_6-DMSO): $[Fe(\mathbf{1})_2](ClO_4)_2$: 3.56−3.63 (m, 1.5H), 3.66−3.74 (m, 4H), 3.77−3.93 (m, 8H), 3.96 (s, 2.5H), 4.08 (s, 2.5H), 4.32 (s, 1.5H), 6.40 (bs, 1.5H), 6.68 (bs, 2H), 7.10−7.35 (m, 11H), 7.45−7.73 (m, 10.5H), 7.82 (d, 1.5H), 7.93 (m, 6H), 8.15 (d, 2H), 8.23 (m, 3.5H), 8.61 (m, 4H), 9.12 (s, 2H), 9.18 (s, 2H); $Co(\mathbf{1})_2(ClO_4)_2$: 3.52−4.15 (m 6H), 4.25 (m, 6.5H), 4.37 (m 3H), 4.55 (t, 1.5H), 4.65 (s, 1.5H), 4.72 (s, 0.5H), 5.02 (s, 1H), 6.35 (m, 1.5H), 6.60 (s, 0.5H), 6.80 (s, 0.5H), 7.15 (m, 1.5H), 7.30 (m, 0.5H), 7.35−7.68 (m 2.5H), 7.75−8.09 (m, 7H), 8.13−8.39 (m, 2.5H), 8.55 (d, 2.5H), 8.68 (bs, 1H), 8.80−9.05 (m, 5H), 9.20 (s, 0.25H), 9.25 (s, 0.25H), 9.38 (bs, 2.5H), 13.63 (m, 3H).

Scheme 3. Structures of Oligopeptides ***1***−***4***

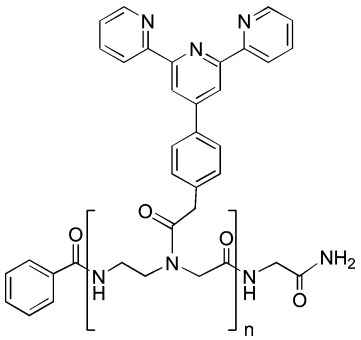

1, 2, 3, 4

Results and Discussion

Metalated Artificial Oligopeptides. To use octahedral metals to form cross-links between artificial oligopeptide strands, the tridentate phenyl terpyridine ligands were incorporated onto the aminoethylglycine scaffold. Following synthesis of the acetic acid phenyl terpyridine ligand (tpy-

ph-CH_2COOH) by acid-catalyzed hydrolysis of the nitrile derivative, this was coupled to the secondary amine of Fmoc-aeg-OtBu·HCl using EDC/HOBt, and the tBu removed by acid hydrolysis to give the new tridentate monomer Fmoc-aeg-(ph-tpy)OH·TFA (Scheme 2). The artificial oligopeptides ***1***−***4*** shown in Scheme 3 were then synthesized using solid-phase peptide synthesis and obtained in yields of 20−40% (Table 1), only slightly lower than those observed for peptide coupling of pyridine-substituted aeg monomers.[9b] Following purification of oligopeptides ***1***−***4*** by preparatory scale HPLC, the purity and identity of the products was confirmed by NMR and positive-ion electrospray mass spectrometry (Table 1).

The ^{1}H NMR spectra yielded the expected relative ^{1}H integrations for each species. However, similar to our pyridine-substituted analogs[15] and PNA[16] structures, the NMR spectra are complicated by the presence of rotamer species. Figure 1 contains a series of ^{1}H NMR spectra obtained at variable temperatures to demonstrate the effect of rotamers on the spectra of ***1***. As the temperature is increased, coalescence of the peaks to the number that is expected (i.e., in the absence of rotamers) is indicative of rotamer structures at low temperature that give rise to chemically nonequivalent ^{1}H with two distinct signals. For example, this is clearly shown between 3.4 and 4.2 ppm, where a series of eight peaks observed at room temperature collapse at high temperature to the five sharp peaks that are expected in this region. The complexity of the room-temperature spectra of the oligopeptides is exacerbated as the oligopeptide length, as well as corresponding number of chemically nonequivalent protons, increases. ^{1}H NMR spectra of ***2***−***4*** therefore consist of broad multiplets that are analyzed by comparison of the ^{1}H integrations: in all cases, the spectra for ***1***−***4*** yield the expected relative (i.e., aromatic and amide vs aliphatic) number of protons. To conclusively confirm their identity and purity, complete assignment of the peaks observed in HMQC spectra (and COSY in the case of ***1***) obtained for ***1***−***4*** was performed (Supporting Information).

Terpyridine ligands are known to chelate Co(II) and Fe(II) to form $[M(tpy)_2]^{2+}$ complexes;[17] addition of Co(II) and Fe(II) to the phenyl terpyridine-substituted oligopeptides was expected to similarly cause formation of six-coordinate metal complexes and form multimetallic supramolecular structures. Therefore, each of the artificial oligopeptides ***1***−***4*** was reacted with $Co(ClO_4)_2$ and $Fe(ClO_4)_2$ in methanolic solutions with the aim of producing the metal-linked peptide duplexes depicted in Scheme 4. Metal complexation was followed by monitoring the change in the absorbance of the solution at wavelengths associated with the metal-to-ligand charge transfer (MLCT) bands for $[Co(ph\text{-}tpy)_2]^{2+}$ (514 nm) and

Scheme 4. Structures of Metalated Oligopeptides ***1***−***4***

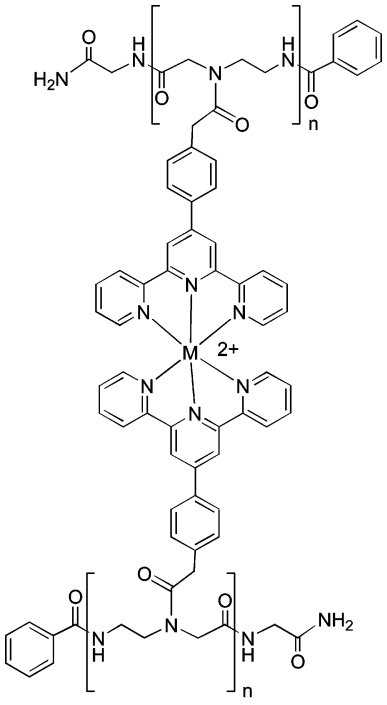

n = 1,2,3,4

M = Co, Fe

$[Fe(ph\text{-}tpy)_2]^{2+}$ (567 nm),[18] as shown in Figure 2. In each case, the MLCT absorbance increased and leveled at values that are consistent with the stoichiometric reaction to make $[M(ph\text{-}tpy)_2]^{2+}$ complexes. The equivalence points were determined from the plots in Figure 2 as described previously.[9b] For example, in the reaction of Co(II) with ***3***, the equivalence point is reached when the molar ratio is 1.5 Co:1 oligopeptide, or 3 Co:2 oligopeptides. The calculated equivalence points for each of the oligopeptides upon reaction with Fe and Co are listed in Table 2. These data do not distinguish between the single-stranded structures, cross-linked peptide duplexes, or polymers that are possible for ***2***−***4***. To analyze the products of these reactions, the titration products were isolated and dried before characterization by spectroscopic and electrochemical methods.

In the case of the Fe and Co complexes with ***1***, in which polymer and intrastrand bond formation is not possible, ESI$^+$ and ^{1}H NMR data were obtained. Similar to the oligopeptide ^{1}H NMR, the metalated species spectra are complicated by the presence of rotamers and further broadened and split by metal complexation and the likely through-space interactions of oligopeptide interstrand proton interactions (see Supporting Information). In the case of the paramagnetic Co(II) complex, the aromatic ligand protons are shifted downfield. Nonetheless, the relative integrations of the ^{1}H NMR spectra of the Co and Fe complexes of ***1*** are consistent with the pure $[M(\mathbf{1})_2]^{2+}$ species; observation of the molecular ion peak in the ESI+ mass spectra additionally identify these products.

(15) McLaughlin, R. L. Penn State University, 2005, unpublished results.
(16) For example: (a) Oleszczuk, M.; Rodziewicz-Motowidlo, S.; Falkiewicz, B. *Nucleosides, Nucleotides Nucleic Acids* **2001**, *20*, 1399−1402. (b) Chen, S. M.; Mohan, V.; Kiely, J. S.; Griffith, M. C.; Griffey, R. H. *Tetrahedron Lett.* **1994**, *35*, 5105−5108.
(17) (a) Rao, J. M.; Hughes, M. C.; Macero, D. J. *Inorg. Chem. Acta* **1976**, *16*, 231−236. (b) Rao, J. M.; Macero, D. J.; Hughes, M. C. *Inorg. Chim. Acta* **1980**, *41*, 221−226.
(18) Amouyal, E.; Mouallem-Bahout, M. *J. Chem. Soc., Dalton Trans.* **1992**, *3*, 509−513.

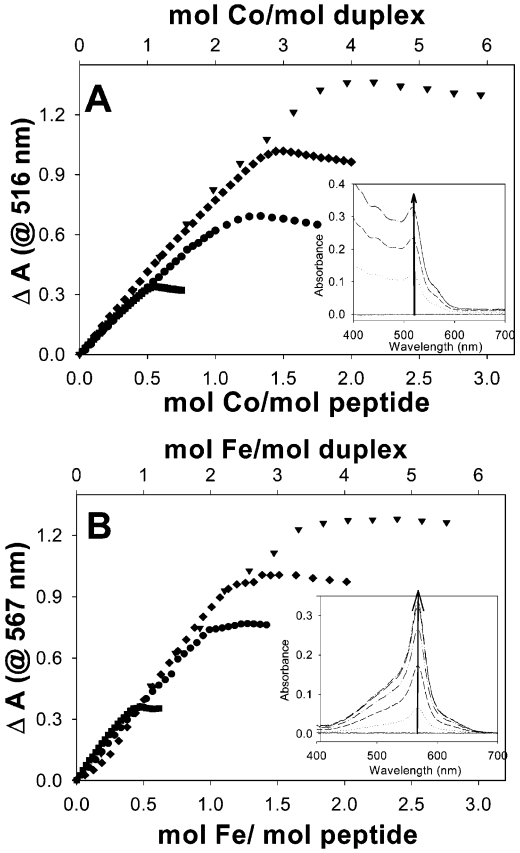

Figure 2. Titration curves for the change in absorbance upon addition of oligopeptide to (A) Co(II) at 514 nm and (B) Fe(II) at 567 nm for oligopeptides (■) ***1***, (●) ***2***, (◆) ***3***, and (▼) ***4*** in methanolic solutions. Insets show representative absorbance difference spectra acquired during titration with ***3***.

Table 2. Solution-Phase Electrochemical Data for Metalated Oligopeptides

		equivalence point[a] (mol metal/mol oligomer)	$E°$ (III/II)[b] (V vs SCE)	ΔE_p[c] (mV)	D ($\times 10^6$)[d] ($cm^2\ s^{-1}$)
Co	***1***	0.50 ± 0.01	0.257	74	9.6 ± 0.1
	2	0.95 ± 0.01	0.266	90	6.2 ± 0.1
	3	1.44 ± 0.01	0.268	99	3.5 ± 0.1
	4	2.0 ± 0.1	0.277	83	2.0 ± 0. 1
Fe	***1***	0.497 ± 0.001	0.979	79	20 ± 1
	2	1.019 ± 0.004	0.991	66	15 ± 1
	3	1.53 ± 0.02	1.01	59	8.6 ± 0.1
	4	2.04 ± 0.09	0.987	36	6.6 ± 0.1

[a] Determined from UV−vis titration curves at 514 and 567 nm for the Co and Fe complexes, respectively. [b] Formal potential of the oxidation reaction, using the average of the oxidative and reductive peak potentials,[11] obtained from cyclic voltammograms acquired at a potential scan rate of 50 mV s^{-1} in 0.15 M TBAP in ACN. [c] Difference in oxidative and reductive peak potentials during cyclic voltammetry as in *b*. [d] Diffusion coefficients obtained from chronocouletry of the charge transients using eq 2.

ESI+ mass spectra were also obtained for the products of the reaction of Fe(II) and Co(II) with oligopeptide ***2***. In each of these cases, the molecular ion peaks (the M^{4+} ion) conclusively identified the product as two cross-linked oligopeptides linked by two metal ions (i.e., $M_2(\boldsymbol{2})_2^{4+}$) to form the dimetallic peptide duplexes.

The ^{1}H NMR spectra for the metal titration products of ***2***−***4*** was overwhelmed by the presence of water even after extended periods of lyophilization (2 weeks). Moreover, we were unable to observe molecular ion peaks in the ESI+ spectra of ***3*** and ***4***. There are two possible explanations for the absence of the molecular ions: (i) the resulting multimetallic duplexes are too unstable in ESI+ conditions to be observed or (ii) the products are polymeric species which are inefficiently ionized (no higher-molecular-weight ions were observed by either ESI+ or MALDI-TOF mass spectrometry). The former of these is an ongoing challenge in the characterization of inorganic supramolecular compounds[19] and is reasonable to expect for the highly charged, larger tri- and tetrametallic structures.

Solution Electrochemistry. To therefore distinguish between duplexes and polymers, we turned to quantitative analysis of their mass transport rates by electrochemical methods. Since metal-linked peptide duplexes would have substantially smaller dimensions than polymeric species, this would lead to their faster mass transport (i.e., diffusion) rates according to the Stokes−Einstein equation:[20]

$$D = k_B T/6\pi\eta a \qquad (1)$$

in which the diffusion coefficient (D) is inversely related to the hydrodynamic radius (a) of the molecule and the viscosity of the medium (η), and where k_B is Boltzman's constant and T is the temperature. Thus, the measured D values in the same solvent are expected to be directly related to changes in the molecular radii.

In unstirred electrochemical solutions, the anodic and cathodic currents can be quantitatively related to D so that this analysis may be made. Figure 3 compares the oxidative cyclic voltammograms obtained for each of the Co(II) and Fe(II) complexes of oligopeptides ***1***−***4***,[21] which have been normalized for the concentration of metal complex. In each case, only a single oxidative wave, which is attributed to either the Co (III/II) at ∼0.26 V or the Fe(III/II) at ∼0.99 V reactions, is observed. The formal potentials ($E°$) of these reactions are listed in Table 2 and appear to slightly increase with increasing oligopeptide length, which could reflect differences in local environment of the metal complexes for the larger structures. However, we simultaneously observe that the longer oligopeptides have sharper wave shapes and the difference between the anodic and cathodic peaks (ΔE_p) decreases, each of which are indicative of adsorption to the electrode surface and could account for the shift in $E°$. Each of the Co species has a larger ΔE_p than their isostructural Fe analogs, which is due to the known slower heterogeneous kinetics for Co(II) oxidations.[22] In all cases, only one oxidative peak is apparent, indicating that there is a lack of

(19) (a) Otto, W. H.; Keefe, M. H.; Splan, K. E.; Hupp, J. T.; Larive, C. K. *Inorg. Chem.* **2002**, *41*, 6172−6174. (b) Jude, H.; Sinclair, D. J.; Das, N.; Sherburn, M. S.; Stang, P. J. *J. Org. Chem.* **2006**, *71*, 4155−4163. (c) Jude, H.; Disteldorf, H.; Fischer, S.; Wedge, T.; Hawkridge, A. M.; Arif, A. M.; Hawthorne, M. F.; Muddiman, D. C.; Stang, P. J. *J. Am. Chem. Soc.* **2005**, *127*, 12131−12139.
(20) Atkins, P.; de Paula J. *Physical Chemistry*, 7th ed.; W.H. Freeman and Co.: New York, 2002.
(21) The need to use water to solubilize the materials precludes observation of the Co(II/I) reduction.
(22) a) Szalda, D. J.; Creutz, C.; Mahajan, D.; Sutin, N. *Inorg. Chem.* **1983**, *22*, 2372−2379. b) Szalda, D. J.; Macartney, D. H.; Sutin, N. *Inorg. Chem.* **1984**, *23*, 3473−3479. c) Gao, Y.; Lipowitz, K. B.; Schultz, F. A. *J. Am. Chem. Soc.* **1995**, *117*, 11932−11938. d) Manchanda, R. *Inorg. Chim. Acta* **1996**, *245*, 91−95. e) De Alwis, D. C. L.; Schultz, F. A. *Inorg. Chem.* **2003**, *42*, 3616−3622.

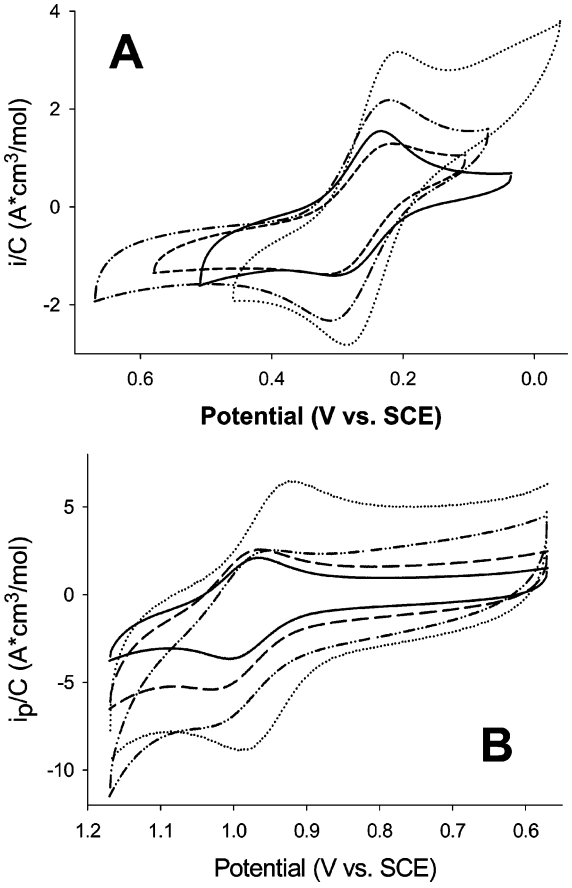

Figure 3. Cyclic voltammograms obtained for solutions containing (A) Co and (B) Fe complexes of the oligopeptides ***1*** (· · ·), ***2*** (· · −), ***3*** (− − −), and ***4*** (−) in 80:20 ACN/H_2O with 0.15 M TBAP supporting electrolyte, acquired at a potential scan rate of 50 mV s^{-1}. Currents are normalized for the metal complex concentrations determined separately from the solution absorbances.

electronic coupling between redox centers, which is expected for metal complexes that are not bridged by conjugated ligands.

The amount of current observed in the cyclic voltammograms in Figure 3 is inversely related to the length of the oligopeptide. Since these data are normalized to the metal complex concentration and these are one-electron oxidations ($n = 1$), the decreased anodic current is a result of slower mass transport to the electrode surface (i.e., $i \propto D^{1/2}$). Analysis of the peak currents (i_p) as a function of the potential scan rate (ν) are consistent with mixed diffusion and electrode adsorption in these experiments,[11] so that this data cannot properly be used to determine D. To accurately measure D of species that tend to adsorb to electrode surfaces, chronocoulometry was used. Application of anodic potential steps to the diffusion-limited portion of the oxidative wave evolves charge (Q) over this time (t) according to[11]

$$Q = (nFAD^{1/2}C/2\pi)t^{1/2} + Q_{dl} + Q_{ads} \qquad (2)$$

where Q_{dl} is the double layer charge and Q_{ads} is the charge contribution from the adsorbed species. The linearized charge

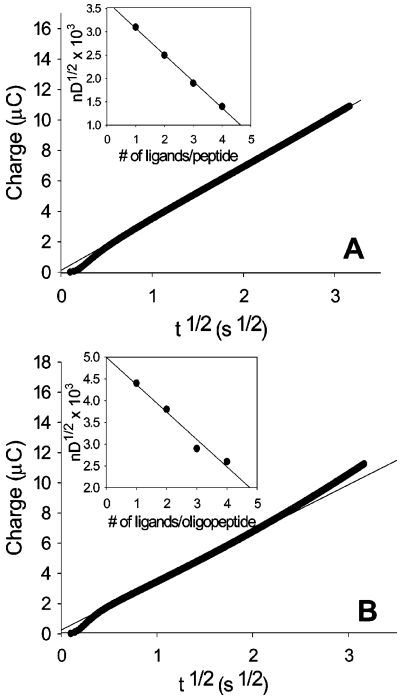

Figure 4. Linearized charge transients of the (A) Co and (B) Fe complexes of ***2*** in 80:20 ACN/H_2O with 0.15 M TBAP. Insets show the calculated $nD^{1/2}$ of the metalated complexes of oligopeptides ***1***−***4*** vs the number of ligands on each strand, with linear regression.

transients for the Fe and Co complexes of ***2*** are shown in Figure 4; the slopes of these lines are used together with the known concentrations of metal complexes to calculate the term $nD^{1/2}$. Since in these cases $n = 1$, the diffusion coefficient of each species is determined and given in Table 2; the measured values of D are within an order of magnitude of mass transport rates of monometallic, small molecule inorganic complexes.[11] In Table 2, the measured D for the Co-containing species are smaller than those measured for the Fe species, which is likely a convolution due to slower heterogeneous kinetics of the Co(III/II) couple. The mass transport rates decrease with increasing oligopeptide length (Figure 4, insets), as predicted by eq 1, and demonstrate that the primary species in solution are metalated oligopeptides are *not* polymeric structures. Using the mass spectra and electrochemical data, a reasonable conclusion is that the majority of the soluble metalated oligopeptides are double-stranded duplex structures and that if any polymeric species form during metal complexation, their relative solution concentrations are not appreciable.

Film Electrochemistry and Spectroelectrochemistry. Since the metalated oligopeptides were found to adsorb to the surface of the working electrode, the electrochemical and spectroelectrochemical properties of these films in the absence of solution-phase species were also investigated. To deposit the films, sequential cyclic voltammograms were performed. The typical response during 20 sequential cycles is shown in Figure 5A for the Fe complex of ***4*** using a Pt working electrode, in which the peak current increases incrementally and ΔE_p decreases as material is deposited onto the electrode. The electrode was then removed from the metalated oligopeptide solution, rinsed thoroughly with ACN,

(23) For example, (a) Belanger, S.; Stevenson, K. J.; Mudakha, S. A.; Hupp, J. T. *Langmuir* **1999**, *15*, 837−843. (b) Sayre, C. N.; Collard, P. A. *Langmuir* **1997**, *13*, 714−722.

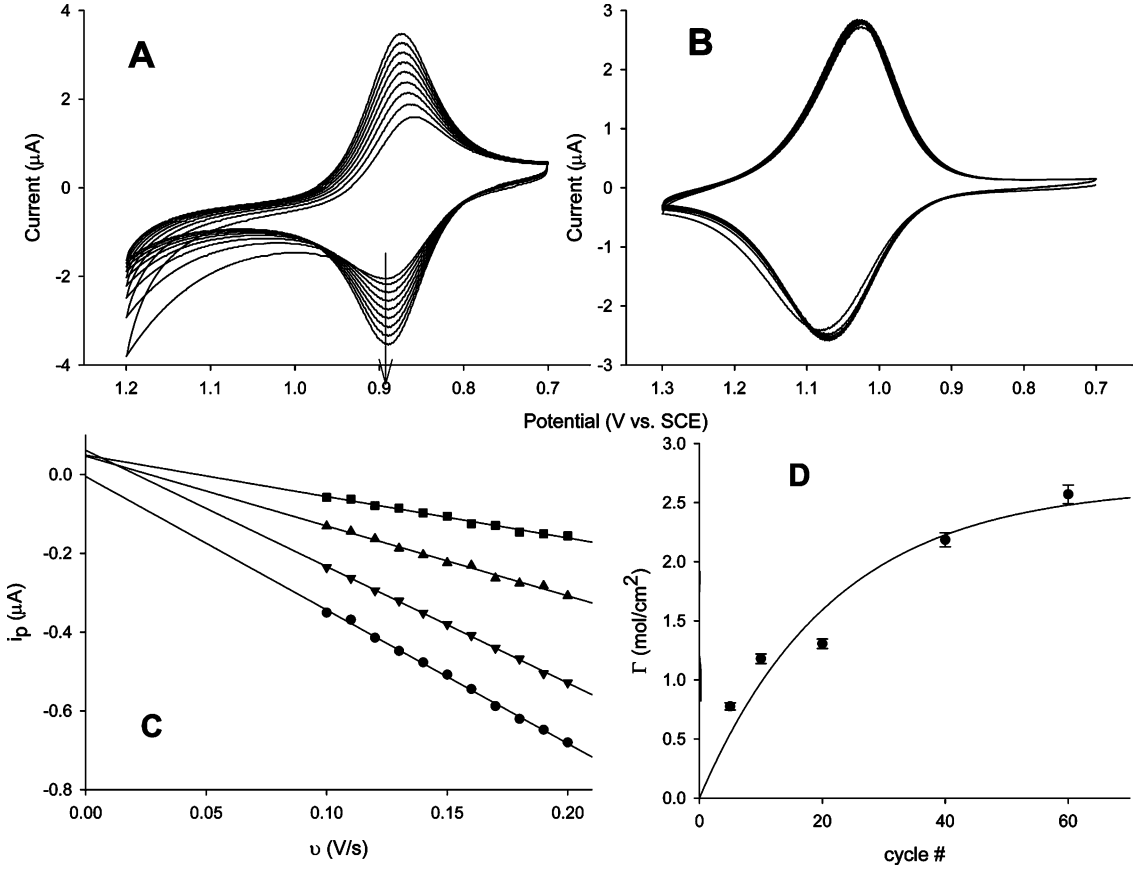

Figure 5. (A) Sequential cyclic voltammograms of $[Fe_4(\boldsymbol{4})_2]^{8+}$ using a Pt electrode and potential scan rate of 50 mV s^{-1}. (B) Cyclic voltammogram of the same film in 0.2 M TBAP in ACN using a scan rate of 50 mV s^{-1}. (C) Peak current vs scan rate for films deposited on a Pt electrode at 50 mV s^{-1} in 0.2 M TBAP ACN solutions following (■) 5, (▲) 20, (▼) 40, and (●) 60 deposition cycles. (D) Surface coverage of metal complexes for $[Fe_4(\boldsymbol{4})_2]^{8+}$ on the Pt electrode as a function of cycle number.

Table 3. Electrochemical Data for Deposited Films on Pt

	$[Co_3(\boldsymbol{3})_2]^{6+}$		$[Co_4(\boldsymbol{4})_2]^{8+}$		$[Fe_3(\boldsymbol{3})_2]^{6+}$		$[Fe_4(\boldsymbol{4})_2]^{8+}$	
no. of cycles[a]	Γ ($\times 10^{11}$)[b] (mol cm^{-2})	ΔE_p[c] (mV)	Γ ($\times 10^{11}$)[b] (mol cm^{-2})	ΔE_p[c] (mV)	Γ ($\times 10^{11}$)[b] (mol cm^{-2})	ΔE_p[c] (mV)	Γ ($\times 10^{11}$)[b] (mol cm^{-2})	ΔE_p[c] (mV)
5	2.25 ± 0.06	49	2.8 ± 0.1	43	8.4 ± 0.3	46	3.2 ± 0.1	30
10	2.88 ± 0.09	55	3.0 ± 0.1	47	93 ± 0.3	33	4.8 ± 0.4	30
20	3.6 ± 0.3	69	3.9 ± 0.1	52	12.0 ± 0.3	33	5.2 ± 0.4	21
40	6.6 ± 0.3	62	4.4 ± 0.4	53	20.4 ± 0.6	36	8.8 ± 0.4	27
60	7.8 ± 0.6	65	4.4 ± 0.4	50	$22. \pm 0.6$	34	10.2 ± 0.4	34

[a] Electrode potential was swept between 0.7 and 1.2 V (Fe complexes) or 0 and 0.5 V (for Co complexes), at a rate of 50 mV s^{-1} using a Pt working electrode. [b] Surface coverage of metal complex, assuming $n = 1$ per complex, determined from the plot of i_p vs scan rate for films deposited on Pt electrodes and immersed in 0.2 M TBAP in ACN solutions. [c] Difference between the anodic and cathodic peak potentials at a scan rate of 200 mV s^{-1} for films on Pt electrodes immersed in 0.2 M TBAP in ACN.

and placed in a solution of ACN containing only 0.2 M TBAP electrolyte. Figure 5B contains the cyclic voltammograms obtained with this electrode: a chemically reversible oxidative wave that is attributed to the Fe(III/II) couple indicates that the $[Fe_2(\boldsymbol{4})_2]^{2+}$ complex is adsorbed and remains electrochemically accessible. Over the course of the repetitive cycles, the magnitude of the current does not decrease, evidence that the adsorbed layer does not desorb from the electrode. In contrast to the voltammograms obtained of the solution-phase species in Figure 3, there is no shift in the formal potential in Figure 5B and the difference in peak potentials is 44 mV. During potential cycling of similar films of the Co and Fe complexes of ***3*** and ***4***, desorption from the electrode was not observed. In contrast, the cyclic voltammetric currents of films of the metal complexes of ***1*** and ***2*** slowly decrease while sequentially cycling the potential as these molecules desorb and diffuse away from the surface. Adsorption is thus a function of the oligopeptide length, and it is likely a result of the decreased solubility in pure ACN for the larger and more highly charged species.

The peak currents continue to increase during sequential cycling in Figure 5A as a result of continued deposition of larger quantities of material onto the electrode surface. We therefore used this approach to deposit a series of films of varying thickness of the $[Fe_4(\boldsymbol{4})_2]^{8+}$ complex on the Pt electrode by controlling the number of potential cycles. In each case, the resulting voltammograms of the modified electrodes revealed adsorbed films that remained adhered to the electrode surface. Figure 5C contains plots of the peak current as a func-

tion of the potential scan rate for a series of films of $[Fe_4(\boldsymbol{4})_2]^{8+}$ deposited for increasing numbers of deposition cycles. In each case, and for all the Co and Fe complexes of ***3*** and ***4***, the plots are linear. The slopes of the lines are used to calculate the surface coverages (Γ) of adsorbed metal complexes (i.e., $n = 1$), which are listed in Table 3 for various cycle numbers for the Co and Fe complexes of ***3*** and ***4***.[11] Figure 5D shows that the surface coverage exponentially increases and levels off (after ~60 cycles). Leveling off may result from decreased conductivity as the film thickness increases by rate-limiting ion transport through the film, and is typical for charged inorganic redox oligomers and polymers.[23]

The ΔE_p values were determined for each of the four film types as a function of cycle number (i.e., surface coverage, Table 3): the values of these are consistent with electrochemically quasi-reversible reactions. The Co species again have larger ΔE_p values than those for the Fe complexes because of the slower heterogeneous kinetics for the Co oxidation. There is no clear trend in ΔE_p as a function of surface coverage for the Fe complexes, although their Co analogues appear to show a slight increase in ΔE_p for thicker films. While the Fe oxidation kinetics are expected to be electrochemically reversible, rates are also related to counterion permeation and diffusion within these films, resulting in the observed quasi-reversible peak splittings. Investigations are currently underway with more ordered systems to further investigate these phenomena.

Films of the metalated complexes of ***3*** and ***4*** could also be deposited irreversibly on optically transparent ITO-coated glass using the same method. The coated slides were then transferred to a cuvette containing 0.2 M TBAP in ACN and counter and reference electrodes and used as the working electrode in UV−vis spectroelectrochemical experiments. The absorbances of the films were measured at the MLCT wavelengths of the Fe complexes as a function of time while the potential was anodically cycled.[24] Representative data obtained from these experiments are shown in Figure 6 for $[Fe_3(\boldsymbol{3})_2]^{6+}$: as the potential of the electrode becomes more positive, a decrease in the absorbance at the MLCT is observed when the overpotential is sufficiently large to generate Fe(III).[25] Upon reversal of the potential, the MLCT absorbance returns to its initial value, a process that is reproducible for many cycles. Thus, electrochemical cycling of the adsorbed films as in Figure 6 does not cause either desorption or chemical reactions that result in observable changes in the electronic spectra. By using the scan rate for the potential sweep to convert from time to potential, absorbance vs potential plots, such as those in Figure 6B, were generated for the species. The hysteresis in the plots again reflects the quasi-reversible kinetics of the oxidation that likely represents both electron and ion diffusion within the films.

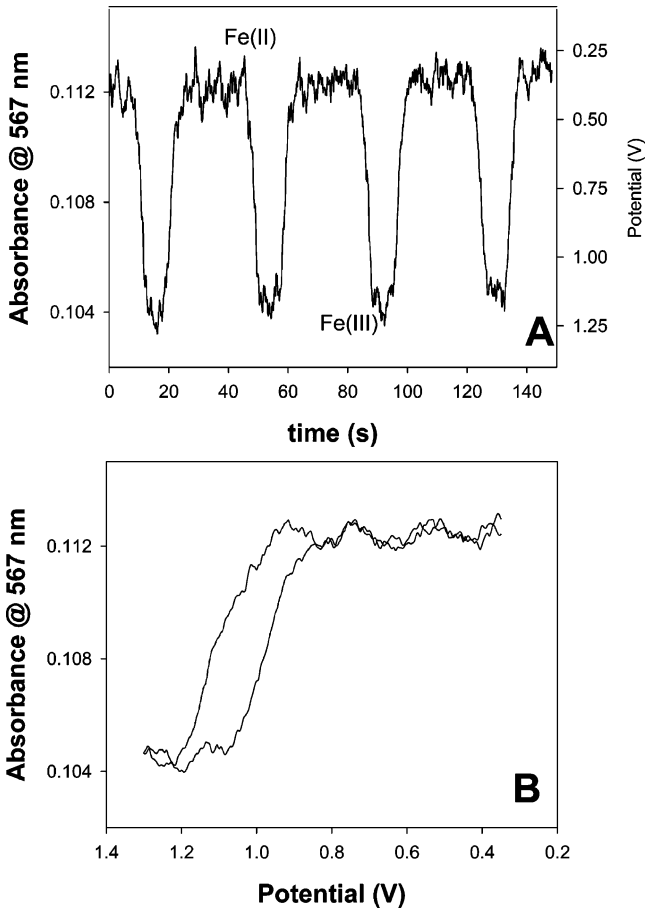

Figure 6. (A) Absorbance at 567 nm for a film of $[Fe_3(\boldsymbol{3})_2]^{6+}$ on ITO-coated glass in 0.2 M TBAP in ACN as the potential is swept from 0.35 to 1.35 V at 50 mV s^{-1}. (B) Absorption of the film at 567 nm as a function of applied potential for one cycle.

Conclusions. This new class of artificial oligopeptides containing pendent tridentate ligands which are crosslinked upon chelation of Co(II) and Fe(II). UV−vis spectrophotometric titrations confirm stoichiometric addition of the metals; the electrochemical data quantitatively demonstrate via measurement of the diffusion coefficients that these are primarily oligopeptide duplex structures. These remain chemically stable, electroactive species that have quasi-reversible to reversible electron-transfer kinetics. The larger metalated oligopeptides form electrodeposited films of controllable surface coverage that enable interrogation by spectroelectrochemical methods. While the kinetics of the Co(II) oxidations appear to be slower than the Fe(II) species, analysis of the electron-transfer kinetics, including assessment of transfers between metal complexes in the same duplex or between duplexes, is precluded because of the interplay of adsorption and counterion transport. This structural motif provides the basis for a new type of multimetallic structure in which one-dimensional electron transport can be controlled and studied. Our ongoing investigations seek to further modify the conditions to better control the structure on the electrode surface and quantitatively measure the operative transport mechanisms.

Acknowledgment. We are grateful to the David and Lucile Packard Foundation and the Alfred P. Sloan Founda-

(24) The lower molar absorptivity of the Co complexes of ***3*** and ***4*** precluded spectroelectrochemical investigation of these films.

(25) (a) Bernhard, S.; Goldsmith, J. I.; Takada, K.; Abruna, H. D. *Inorg. Chem.* **2003**, *42*, 4389−4393. (b) Li, H.; Li, Y.; Li, J.; Wang, E.; Dong, S. *Electroanalysis* **1995**, *7*, 742−745.

tion for generous support of this work. K.O. acknowledges support as a Penn State University Graduate Fellow.

Supporting Information Available: Supporting information including ^{1}H NMR spectra of ***1***−***4***, Co(***1***)$_2$, and Fe(***1***)$_2$, HMQC spectra of ***1***−***4***, and COSY of ***1***. This material is available free of charge via the Internet at http://pubs.acs.org.

IC0612101